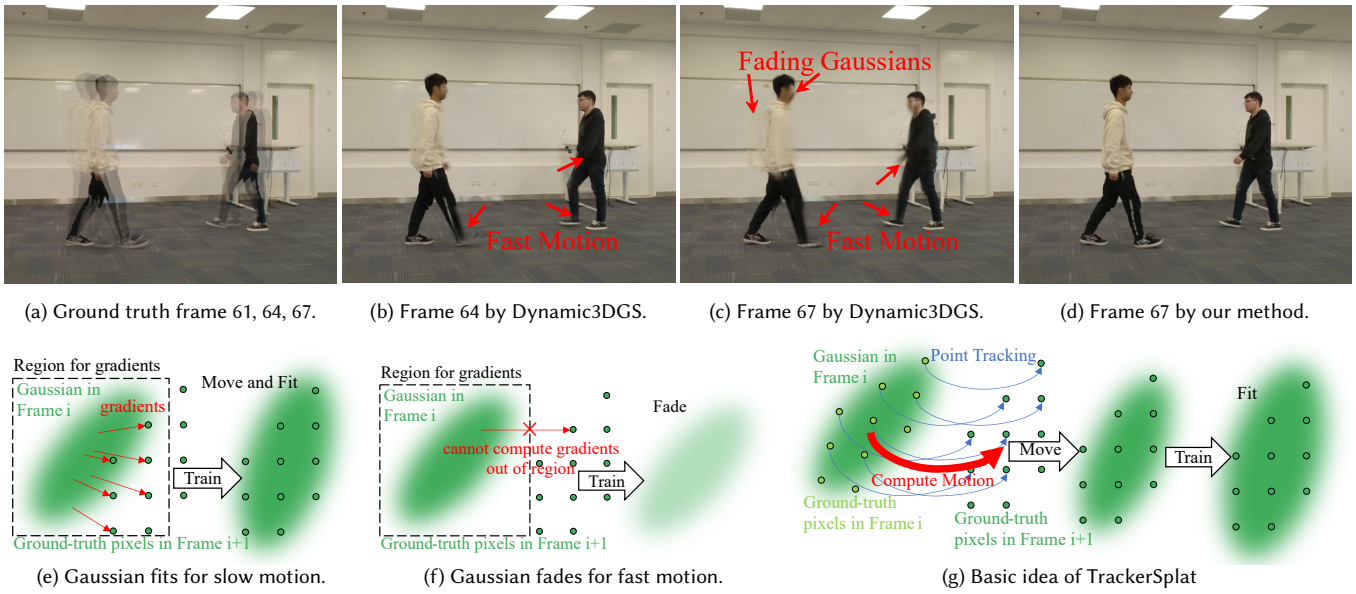


1 TrackerSplat: Exploiting Point Tracking for Fast and Robust Dynamic 3D 2 Gaussians Reconstruction

3 ANONYMOUS AUTHOR(S)

4 SUBMISSION ID: 1094



29 Fig. 1. Illustration of the motivation and basic idea of TrackerSplat. (a) Ground truth from the "walking" sequence. (b), (c) Rendered frames 64 and 67, trained
30 1000 iterations from frame 61 with the physically-based regularization losses introduced by Dynamic3DGS [Luiten et al. 2024]. Gaussians struggle to accurately
31 follow the fast moving object, resulting in fading or incorrect recoloring. (e) Slow motion: object remains in the region for gradient computing, allowing
32 Gaussians to maintain consistent color and follow the movement of object. (f) Fast motion: the object moves outside the region for gradient computing,
33 position gradients fail to align with the movement of object, causing Gaussians to either fade or incorrectly recolor. (d), (g) TrackerSplat to adjust Gaussian
34 position, rotation and scaling parameters according to point tracking results before training, enabling stable and robust training for fast-moving objects.

35 Recent advancements in 3D Gaussian Splatting (3DGS) have demonstrated
36 its potential for efficient and photorealistic 3D reconstructions. However,
37 current Gaussian-based methods for dynamic scene reconstruction struggle
38 with large inter-frame displacements, leading to artifacts and temporal
39 inconsistencies under fast object motions. To address this, we introduce
40 *TrackerSplat*, a novel method that integrates advanced point tracking meth-
41 ods to enhance the robustness and scalability of 3DGS for dynamic scene
42 reconstruction. TrackerSplat utilizes off-the-shelf point tracking models to
43 extract pixel trajectories and triangulate per-view pixel trajectories onto
44 3D Gaussians to guide the relocation, rotation, and scaling of Gaussians be-
45 fore training. This strategy effectively handles large displacements between
46 frames, dramatically reducing the fading and recoloring artifacts prevalent in
47 prior methods. By accurately positioning Gaussians prior to gradient-based
48 optimization, TrackerSplat overcomes the quality degradation associated
49 with large frame gaps when processing multiple adjacent frames in parallel
50 across multiple devices, thereby boosting reconstruction throughput while
51 preserving rendering quality. Experiments on real-world datasets confirm
52 the robustness of TrackerSplat in challenging scenarios with significant
53 displacements, achieving superior throughput under parallel settings and
54 maintaining visual quality compared to baseline methods.

55 CCS Concepts: • Computing methodologies → Rendering; Image-based
56 rendering.

57 Additional Key Words and Phrases: Dynamic Scene, Gaussian Splatting

1 INTRODUCTION

Reconstructing dynamic 3D scenes and generating photo-realistic, temporally consistent renderings have long been fundamental goals in computer vision and graphics. These capabilities are increasingly important for creating controllable, editable, high-quality 3D content, underpinning applications in film, gaming, and the metaverse [Zhang et al. 2021]. Beyond visual fidelity for human audiences, accurately modeling the dynamic 3D environments, including tracking the positions and actions of objects in the scene, also plays a critical role in transformative applications such as robotics [Abou-Chakra et al. 2024], autonomous driving [Zhou et al. 2024]. Despite significant recent advances, efficient and accurate reconstruction of dynamic scenes remains challenging due to the complexities introduced by temporal dynamics and diverse motion patterns.

Recent progress in 3D reconstruction has been driven notably by the success of 3D Gaussian Splatting (3DGS)[Kerbl et al. 2023] for its ability to efficiently represent 3D scenes with photorealism. By modeling 3D space with ellipsoids ("Gaussians"), 3DGS enables intuitive editing through manipulation of individual Gaussians, making it suitable for dynamic scene representation. Building on its strengths,

recent research has adapted 3DGS to dynamic scenarios by explicitly encoding Gaussian parameters as temporal trajectories [Li et al. 2024a; Lin et al. 2024; Zhao et al. 2024] or by representing motion fields using implicit features [Huang et al. 2024; Li et al. 2024c,b; Wu et al. 2024]. These methods typically rely on frame-to-frame adaptation, iteratively refining Gaussian parameters by training on consecutive frames to ensure smooth temporal transitions [Gao et al. 2024; Luiten et al. 2024; Sun et al. 2024].

Despite these advancements, the reconstruction process of 3DGS is computationally intensive, limiting its application in scenarios demanding both high quality and high throughput, such as live streaming and interactive virtual environments. To improve the throughput of reconstruction without adding end-to-end latency, a natural solution is to process multiple adjacent frames in parallel across multiple GPUs. However, our experiments reveal that existing methods suffer from significant quality degradation when handling large displacements between frames, leading to visible artifacts, as is shown in Figure 1b and Figure 1c.

Upon further analysis, we identify a critical issue in 3DGS that contributes to this quality degradation. Existing approaches rely heavily on fine-tuning Gaussian parameters from frame to frame using iterative training. A core idea behind these methods is to guide Gaussian motion using position gradients computed by comparing Gaussian colors with the surrounding pixels they overlap (Figure 1e). Due to computational constraints, gradient computations are restricted to a limited local neighborhood. This constraint results in inaccurate position gradients when objects experience significant inter-frame motion and move outside this restricted region (Figure 1f). In parallel setups, increased parallelism widens the frame gaps assigned to each device, amplifying the likelihood of significant object displacements and consequently exacerbating this issue, leading to prominent artifacts (Figure 1c).

To mitigate this limitation, we propose directly estimating Gaussian trajectories across frames rather than relying solely on the gradient to update their positions. Recent advancements in point tracking [Karaev et al. 2024, 2025] provide robust pixel-level motion estimation across video frames. However, integrating point tracking presents two key challenges: (1) translating 2D pixel trajectories into updates for 3D Gaussian parameters, and (2) mitigating inaccuracies in pixel trajectories to prevent error accumulation during updates.

We introduce *TrackerSplat* to address these challenges. As illustrated in Figure 1g, TrackerSplat integrates an off-the-shelf point tracking model to capture pixel trajectories for each viewpoint. To compute updates for 3D Gaussians, we propose Parallel Weighted Incremental Least Squares (PWI-LS) that derives 2D motion from pixel trajectories. These 2D motions from multiple views are triangulated to update Gaussian positions, rotations, and scales. To reduce inaccuracies, the computed updates are smoothed by Motion Regularization, and Gaussian parameters are further refined through training. By repositioning Gaussians closer to their correct locations before training, TrackerSplat maintains coherent tracking despite large displacements, significantly reducing fading or recoloring artifacts observed in prior methods. Most importantly, since tracking mitigates the impact of large frame gaps, TrackerSplat enables independent frame updates across multiple GPUs, thus increasing reconstruction throughput without sacrificing quality.

To the best of our knowledge, we are the first to identify the robustness limitations of 3DGS in handling large inter-frame displacements, and TrackerSplat is the first method to directly compute Gaussian trajectories using multi-view point tracking results to address this limitation. While prior works have incorporated tracking within Gaussian-based pipelines [Lei et al. 2024; Stearns et al. 2024; Wang et al. 2024], direct use of multi-view point tracking for trajectory estimation remains unexplored.

We implement TrackerSplat with a parallel pipeline across 8 GPUs and evaluate it on real-world dynamic scene datasets. Our extensive experiments demonstrate superior throughput under parallel settings, while preserving or improving visual quality compared to baseline methods. Our findings confirm the effectiveness of incorporating point tracking into 3DGS-based dynamic reconstruction, paving the way for scalable, accurate, and temporally consistent dynamic 3D scene reconstructions.

2 RELATED WORK

2.1 3D Gaussian Splatting for Dynamic Scenes

Recent years have witnessed significant progress in reconstructing 3D representations from multi-view captures. Among these advancements, 3D Gaussian Splatting (3DGS) [Kerbl et al. 2023] has emerged as a leading approach. 3DGS represents scenes using a set of ellipsoids ("Gaussians") and achieves photorealistic rendering with high efficiency. Building on its success, recent studies have extended 3DGS to dynamic scenarios. Some methods dynamically add or remove Gaussians to represent motion through their appearance and disappearance [Duan et al. 2024; Sun et al. 2024]. However, this approach may lead to significant storage overhead due to the large number of Gaussians needed to capture the dynamic nature of the scene. To address this, other methods explicitly represent dynamic scenes using Gaussians and their trajectories, significantly reducing the number of Gaussians. For instance, some approaches use implicit features conditioned on time to represent motion fields [Huang et al. 2024; Li et al. 2024b,a; Lin et al. 2024; Zhao et al. 2024], while others adopt triplane representations for higher spatial and temporal resolutions [Wu et al. 2024]. Recent advancements also include frame-to-frame adaptation techniques, where Gaussian parameters are iteratively refined by training on consecutive frames [Gao et al. 2024; Luiten et al. 2024; Xu et al. 2024; Yang et al. 2023].

2.2 Point Tracking

Point tracking identifies the position and visibility of specific pixels across video sequences [Harley et al. 2022; Seidenschwarz et al. 2025; Wang et al. 2023], providing robust trajectory estimation even under challenging conditions such as occlusion. Recently, point tracking has attracted considerable attention within the computer vision community. Empowered by semi-supervised correspondence [Shrivastava and Owens 2025], CoTracker [Karaev et al. 2024, 2025] achieves state-of-the-art sparse tracking performance, while DOT [Le Moing et al. 2024] further enhances dense tracking accuracy and efficiency. Point tracking has been used in 3D reconstruction, especially for reconstructing dynamic scenes from monocular videos [Lei et al. 2024; Stearns et al. 2024; Wang et al. 2024]. In these methods, point tracking typically separates static background from dynamic foreground

or serves as a regularization term for dynamic regions. However, the direct application of point tracker results to compute 3D Gaussian splatting parameters for multi-view dynamic scene reconstruction remains largely unexplored.

3 PRELIMINARIES

3.1 Mathamatical Reperesentation of 3D Gaussians

3DGS represents the scenes with 3D Gaussians. Each 3D Gaussians is characterized by two key components: its mean μ_{3D} represents the position of the ellipsoid, and its covariance matrix $\Sigma_{3D} = RSS^\top R^\top$, composed of a scaling matrix S and a rotation matrix R , describes the spread and orientation of the Gaussian ellipsoid respectively.

When projected onto the 2D image plane, the 3D Gaussian becomes a 2D Gaussian distribution. Concretely, for a point on the image plane, the density function of the 2D Gaussian distribution can be represented as:

$$\begin{aligned} G(\mathbf{x}) &= e^{-\frac{1}{2}(\mathbf{x}-\mu_{2D})^\top \Sigma_{2D}^{-1} (\mathbf{x}-\mu_{2D})} \\ \Sigma_{2D} &= JW\Sigma_{3D}W^\top J^\top \\ \mu_{2D} &= \frac{1}{z}PW\mu_{3D} \end{aligned} \quad (1)$$

where J is the Jacobian of the affine approximation of the projective transformation, W is the viewport transformation matrix, P is the projection transformation matrix, and z is the depth value in $PW\mu_{3D}$. After projection, the color of each pixel is calculated by alpha-blending each Gaussian according to its depth.

3.2 Integration of Point Tracking

To track 3D Gaussians, we rely on point tracking in video frames captured from multiple viewpoints. In particular, we employ Dense Optical Tracking (DOT) [Le Moing et al. 2024], a simple yet efficient method for point tracking. For each pixel i located at position \mathbf{x}_i in the first frame, point tracking estimates its corresponding position ($\mathbf{x}_i \mapsto \mathbf{x}'_i$) in any subsequent target frame.

4 METHOD

4.1 Overview

We provide an overview of TrackerSplat in Figure 2. Our goal is to reconstruct dynamic scenes from video clips captured from multiple fixed viewpoints by tracking and refining a set of Gaussian representations. Our methods can be divided into four stages:

Initialization. For the first frame, we initialize 3D Gaussians using existing reconstruction methods for static scenes, such as InstantSplat [Fan et al. 2024].

Point Tracking. For each subsequent frame, we employ a point tracking model to extract 2D trajectories for every pixel in the initial frame throughout the video clip.

Motion Compensation. In this stage, we compute the updated parameters of the 3D Gaussians based on the point tracking results. TrackerSplat first solves the Gaussian motions (Sec. 4.2) on the 2D image plane using *Parallel Weighted Incremental Least Squares* (PWI-LS) (Sec. 4.3) and then *updates Gaussians from multi-view observations* (Sec.4.4). To mitigate the impact of errors from point tracking and PWI-LS on quality, we introduce *Motion Regularization*

(Sec. 4.5), which applies median filtering and propagates motion information according to neighboring Gaussians.

Refinement. Finally, we refine the parameters of each frame by training on the input video clips (Sec. 4.6).

In this section, we detail each step of the proposed approach and show how they can be parallelized on multi-GPU devices with our *Parallel Pipeline* (Sec. 4.7).

4.2 Definition of Gaussian Motion

To serve as the basis for tracking 3D Gaussians across multiple video viewpoints, it is necessary to define the motion of a 2D Gaussian distribution on the image plane. Consider a 2D Gaussian distribution $G(\mathbf{x})$ on a specific image plane in the first frame, characterized by its covariance Σ_{2D} and mean μ_{2D} . We define the motion of this Gaussian as an affine transformation $[A|b]$, which maps $G(\mathbf{x})$ to a new 2D Gaussian distribution $G'(\mathbf{x})$ in a subsequent frame. Formally, $G(\mathbf{x}) = G'(A\mathbf{x} + b)$. Under this affine transformation, the updated mean μ'_{2D} and covariance Σ'_{2D} can be derived as follows:

$$\begin{aligned} \Sigma'_{2D} &= A\Sigma_{2D}A^\top \\ \mu'_{2D} &= A\mu_{2D} + b \end{aligned} \quad (2)$$

4.3 Parallel Weighted Incremental Least Squares (PWI-LS)

4.3.1 Problem Formulation. Let $\{\mathbf{x}_i\}, i \in [1, n]$ denote the collection of pixels on a specific image plane covered by the 2D Gaussian in the first frame. Our goal is to find the affine transformation $[A|b]$ that best aligns these pixel coordinates \mathbf{x}_i with their tracked positions \mathbf{x}'_i in the subsequent frame. This can be formulated as follows:

$$\min_{A,b} \sum_{i=1}^n \|A\mathbf{x}_i + b - \mathbf{x}'_i\|^2$$

4.3.2 Naive Least Squares. A straightforward method to solve this optimization is through least squares. By stacking all point pairs $(\mathbf{x}_i \mapsto \mathbf{x}'_i)$ into matrices X and Y , the affine transformation $[A|b]$ can be computed as:

$$\begin{aligned} [\hat{A}|\hat{b}] &= (X^\top X)^{-1} X^\top Y \\ X &= \begin{bmatrix} x_1 & \dots & x_i & \dots & x_n \end{bmatrix}^\top \\ Y &= \begin{bmatrix} x'_1 & \dots & x'_i & \dots & x'_n \end{bmatrix}^\top \end{aligned} \quad (3)$$

However, in cases where many pixels fall under each Gaussian and when multiple Gaussians overlap, explicitly constructing and inverting these large matrices per Gaussian is computationally expensive. This motivates a more efficient, incremental approach.

4.3.3 Incremental Least Squares. To mitigate high computational costs, we exploit the additive structure of $X^\top X$ and $X^\top Y$ in Equation 3 and decompose them into per-pixel contributions:

$$\begin{aligned} X^\top X &= \sum_{i=1}^n P_i = \sum_{i=1}^n \begin{bmatrix} x_i \\ 1 \end{bmatrix} \cdot [x_i^\top, 1] \\ X^\top Y &= \sum_{i=1}^n Q_i = \sum_{i=1}^n \begin{bmatrix} x_i \\ 1 \end{bmatrix} \cdot x_i'^\top \end{aligned}$$

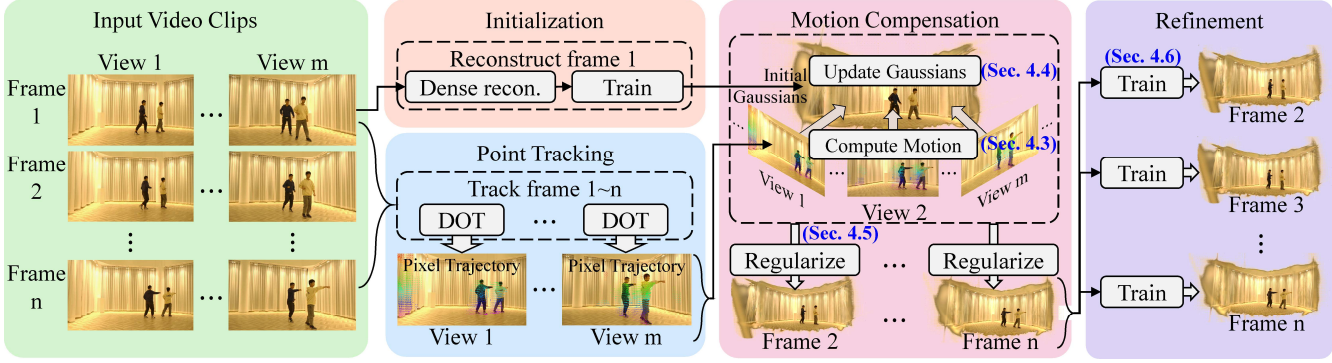


Fig. 2. TrackerSplat Overview. Our method processes video clips captured from multiple fixed viewpoints. It begins by applying existing reconstruction techniques to initialize a set of 3D Gaussians for the first frame. For subsequent frames, the position, rotation, and scale of these Gaussians are updated based on point tracking across views, with their motions regularized by neighboring Gaussians. Finally, the Gaussian parameters of each frame are refined by training on input frames.

By expressing the solution as sums of P_i and Q_i , the contribution of each pixel can be handled independently. This incremental scheme avoids building full matrices for all pixels, allowing us to accumulate partial results P_i and Q_i in parallel, paving the way for efficient parallel implementations.

4.3.4 Weighted Least Squares. In regions of partial coverage (e.g., object boundaries with overlapping foreground/background Gaussians), unweighted alignment can be misled by pixels that do not truly belong to a particular motion. For example, consider a static background Gaussian and a high-density moving Gaussian in front of it. The moving Gaussian may partially cover a moving pixel with very high opacity, and a static pixel with very low opacity. In this situation, the static pixel should not contribute to the motion of the moving Gaussian. To achieve this, we adopt a weighted formulation:

$$\begin{aligned} [\hat{A}|\hat{b}] &= V_1^{-1}V_2 \\ V_1 &= \sum_{i=1}^n w_i P_i \quad V_2 = \sum_{i=1}^n w_i Q_i \end{aligned} \quad (4)$$

where each pixel carries a weight w_i representing the likelihood that its motion corresponds to a particular Gaussian. In our implementation, w_i is set to $\alpha_i T_i$, where α_i and T_i are the opacity and the transparency of Gaussian at the pixel i in alpha-blending. This ensures that boundary pixels with low opacity contribute less to the accumulated statistics, thereby reducing sensitivity to irrelevant motions from overlapping regions.

4.3.5 Acceleration by GPU. The Weighted Incremental Least Squares algorithm can be optimized for GPU execution to exploit its parallel processing capabilities for acceleration, which results in the *Parallel Weighted Incremental Least Squares* algorithm:

For each Gaussian, we allocate GPU memory for the (3×3) matrix V_1 and the (3×2) matrix V_2 . We modify the rendering process to compute V_1 and V_2 , where the $w_i P_i$ and $w_i Q_i$ are computed in parallel and aggregated by atomic addition into the corresponding V_1 and V_2 . After processing all pixels, the motion $[\hat{A}|\hat{b}]$ of each Gaussian are computed by Equation 4 to obtain affine transformation

$[A|b]$ of each Gaussian. To avoid numerical instability, we discard the motion of Gaussians that cover fewer than three pixels, or have a near-singular matrix V_1 .

4.4 Update Gaussians from Multi-view Observations

Once we have motion $[A|b]$ of each Gaussian in multiple views, we can compute its updated covariance matrix Σ'_{2D} and 2D mean μ'_{2D} according to Equation 2, and then the updated 3D covariance matrix Σ'_{3D} and 3D mean μ'_{3D} can be derived from the multi-view 2D means and covariance.

4.4.1 Compute 3D Mean. Determining the 3D mean μ'_{3D} from the 2D means μ'_{2D} across multiple views is a typical triangulation problem. With known camera intrinsic and extrinsic, at least two viewpoints are required to compute the μ'_{3D} of a Gaussian. We solve this triangulation problem using Singular Value Decomposition (SVD). To maintain numerical stability, results are discarded for Gaussians observed in fewer than three views or those with low accumulated alpha values.

4.4.2 Compute 3D Covariance Matrix. Given the covariance matrices Σ'_{2D} from multiple views and the parameters J and W of these views, the relationship $\Sigma'_{2D} = JW\Sigma'_{3D}W^\top J^\top$ in Equation 1 yields a linear system in Σ'_{3D} . Each Σ'_{2D} contributes three constraints, while Σ'_{3D} has six unknown parameters. Hence, at least two distinct views are required to solve for Σ'_{3D} .

4.4.3 Decompose Covariance into Rotation and Scale. According to Equation 1, the 3D covariance matrix Σ_{3D} comprises a rotation matrix R and a scaling matrix S . To update these parameters, we perform eigen decomposition on the modified covariance matrix Σ'_{3D} , extracting the updated rotation matrix R' and scaling matrix S' . In eigen decomposition, the eigenvector matrix corresponds to the rotation matrix, while the eigenvalues represent the squared scaling matrix.

However, naively using eigen decomposition can lead to two problems: 1) Negative eigenvalues cannot be square-rooted, making them unsuitable for computing the scaling matrix. 2) Eigenvalues

457 are sorted from largest to smallest, which can disrupt the consistent
 458 order of rotation vectors and scaling factors between frames. This
 459 inconsistency can cause adjacent regions to appear to have simi-
 460 lar relative rotations but significantly different rotation matrices,
 461 leading to instability in subsequent motion propagation.

462 To resolve these issues, we discard those Σ'_{3D} with negative eigen-
 463 values, and reorder the eigenvalues and corresponding eigenvectors
 464 to ensure their magnitudes match the order from the first frame.
 465

466 4.5 Motion Regularization

467 Pixel tracking and partial observations can introduce outlier Gaussians
 468 or wrong motions, leading to noticeable deviations. We intro-
 469 duce a motion regularization to address these issues. Specifically, we
 470 apply median filtering based on K-nearest neighbors to smooth the
 471 motion and then propagate the motion to the neighbor Gaussians
 472 that are not determined to be static.
 473

474 **4.5.1 Median Filtering.** We observe that the majority of Gaussians
 475 are stable but a few are outliers. This situation is similar to salt-and-
 476 pepper noise in image processing. Therefore, we heuristically apply
 477 a median filtering approach. Take $\Delta\mu_{3D} = \mu'_{3D} - \mu_{3D}$, $\Delta R = R' - R$,
 478 and $\Delta S = S' - S$ as the difference of a Gaussian between its first
 479 frame. For each Gaussian, we find its K nearest neighbors in 3D
 480 space, and then compute the median of their $\Delta\mu_{3D}$, ΔR , and ΔS and
 481 add these median values to the Gaussian parameters for the update.
 482

483 **4.5.2 Propagation.** The motion of certain Gaussians may not be
 484 reliably determined, for example, due to low visibility (e.g., low
 485 opacity or visible in too few views) or negative eigenvalues arising
 486 from eigen decomposition. For these Gaussians, we apply the motion
 487 propagation that propagates the motion from their neighbor
 488 to them. Before propagation, we first figure out those static Gaussians
 489 by checking whether the pixels they cover are moving or not.
 490 Specifically, we treat the pixels with the movement $|x'_i - x_i|$ given by
 491 the point tracking model as less than 1 pixel as static pixels, count
 492 them, and accumulate their alpha for each Gaussian in the rendering
 493 process. The rule for detecting the static Gaussians can be varied.
 494 In this paper, we take those Gaussians hit by more than 9 pixels
 495 and have more than 90% of its pixels fixed in at least 2 views as
 496 static Gaussians, discard their computed motion, and exclude them
 497 from the motion propagation. We then compute the average of their
 498 $\Delta\mu_{3D}$, ΔS and an average of rotations ΔR in Euler angle form and
 499 add these median values to the Gaussian parameters μ_{3D} , S and R .
 500

501 4.6 Refinement

502 Even with point tracking and multi-view constraints, errors may
 503 persist in the recovered Gaussians. We hence run a final refine-
 504 ment step by training the Gaussian parameters with the input video
 505 frames. As the Gaussians have been moved to an approximately
 506 right position, the training process would be very fast and stable.
 507

508 4.7 Parallel Pipeline

509 As illustrated in Figure 3, three key stages of TrackerSplat can be
 510 executed in parallel. Since our point tracking operates per video clip,
 511 the point tracking can be parallelized by processing video from each
 512 view independently. Additionally, the Motion Compensation and
 513

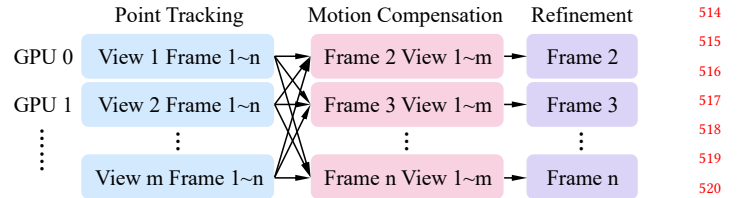


Fig. 3. TrackerSplat Parallel Pipeline.

514 Refinement are both per-frame operations, they can be parallelized
 515 by processing each frame independently, only depending on the
 516 results of Point Tracking and initialization of the first frame. The
 517 parallel pipeline can be implemented on multi-GPU systems and
 518 significantly improve the throughput of TrackerSplat.
 519

520 5 EXPERIMENTS

521 5.1 Datasets

522 We evaluate our method on four widely-used dynamic scene datasets:
Meeting Room dataset [Li et al. 2022a] includes 4 scenes, each of
 523 300 frames captured from 13 viewpoints at a resolution of 1280×720.
Neural 3D Video Synthesis (N3DV) dataset [Li et al. 2022b] contains 6 scenes, each of 300 frames captured from 18 views at
 524 2704×2028 resolution.
Dynamic3DGS dataset [Luiten et al. 2024] comprise 6 scenes (150
 525 frames each) captured from 27 views at 640×360 resolution.

526 **st-nerf** dataset [Zhang et al. 2021] consists of 3 scenes, each contains
 527 75–100 frames from 15 views at 1920×1080 resolution.
 528

529 We use these datasets in two experiment setups:
Short-clip experiments: Videos are segmented into non-overlapping
 530 clips of 3, 5, or 9 frames. The first frame of each clip is reconstructed
 531 in the initialization stage, and subsequent frames are processed in
 532 parallel using 2, 4, or 8 GPUs, respectively. This setup evaluates
 533 quality degradation caused solely by increased parallelism without
 534 cumulative errors across clips.
Long-video experiments: Clips are sequentially connected, with
 535 the last frame of each clip serving as the first frame of the next. Only
 536 the first frame of the first clip is reconstructed in the initialization
 537 stage. This setup evaluates robustness and temporal consistency
 538 over longer sequences.

539 5.2 Implementation Details

540 We carefully evaluated various hyperparameter settings and selected
 541 those achieving the best balance between quality and efficiency.

542 **Initialization.** Following InstantSplat [Fan et al. 2024], we initial-
 543 ize Gaussians from COLMAP point clouds and optimize Gaussian
 544 parameters for 10,000 iterations, providing a stable starting point
 545 for subsequent frames.
 546

547 **Point Tracking.** We use DOT [Le Moing et al. 2024] for pixel track-
 548 ing. We evaluated DOT, CoTracker family [Karaev et al. 2024, 2025],
 549 and TAPIR [Doersch et al. 2023], and found DOT and CoTracker3
 550 consistently delivered superior results. DOT was finally selected
 551 due to its faster speed and lower memory usage. Input images are
 552 resized (Meeting Room: 640×360, N3DV: 800×600, st-nerf: 960×540,
 553 Dynamic3DGS: 640×360) to improve efficiency.
 554

555 556 557 558 559 560 561 562 563 564 565 566 567 568 569 570

571 Table 1. Quantitative comparison of average visual quality ($PSNR \uparrow / SSIM \uparrow / LPIPs \downarrow$) in short-clip experiments under varying GPU parallelism settings (2, 4,
 572 and 8 GPUs). Our method achieves better visual quality in most cases and demonstrates greater robustness than baseline methods as parallelism increases.
 573 Results for all other scenes are included in the supplementary material.

574 Method	575 GPUs	576 "basketball"	577 "boxes"	578 "juggle"	579 "stepin"	580 "vrheadset"	581 "taekwondo"	582 "coffee martini"
P. ST-4DGS	2	30.2 / .936 / .081	30.4 / .944 / .066	31.0 / <u>.951</u> / <u>.063</u>	32.1 / .947 / .071	32.2 / .950 / .067	35.0 / .971 / .027	27.6 / .920 / .110
P. 4DGS	2	30.7 / .940 / <u>.073</u>	30.2 / .941 / .068	30.6 / .947 / .066	32.6 / .950 / <u>.068</u>	32.4 / .950 / .066	35.5 / .974 / .024	27.4 / .918 / .113
P. Dy.3DGS	2	30.2 / .936 / .083	31.3 / <u>.949</u> / <u>.063</u>	31.4 / .951 / .064	32.2 / .947 / .072	32.0 / .950 / .067	36.4 / .977 / .023	27.6 / .918 / .113
P. HiCoM	2	<u>31.0</u> / <u>.940</u> / .080	<u>31.6</u> / .948 / .066	<u>31.9</u> / .951 / .065	<u>32.8</u> / <u>.951</u> / .068	<u>32.8</u> / <u>.953</u> / <u>.065</u>	<u>36.7</u> / .978 / <u>.021</u>	28.0 / <u>.919</u> / .113
Ours	2	32.6 / .950 / .067	32.2 / .953 / .061	32.7 / .956 / .059	32.9 / .953 / .065	33.0 / .954 / .062	36.8 / <u>.977</u> / .021	<u>27.9</u> / .919 / <u>.112</u>
P. ST-4DGS	4	29.7 / .932 / .089	30.2 / .943 / .069	31.0 / .949 / .066	31.9 / .946 / .074	31.9 / .949 / .068	28.4 / .778 / .172	27.5 / .919 / .111
P. 4DGS	4	30.0 / .932 / <u>.082</u>	30.1 / .944 / .068	30.9 / <u>.950</u> / .066	32.6 / <u>.950</u> / <u>.068</u>	32.0 / .949 / .068	34.8 / .972 / .028	27.4 / .917 / .114
P. Dy.3DGS	4	29.1 / .927 / .096	30.8 / .946 / <u>.068</u>	30.8 / .946 / .071	31.7 / .945 / .075	31.5 / .948 / .070	35.8 / .975 / .026	27.6 / .918 / .114
P. HiCoM	4	<u>30.4</u> / <u>.936</u> / .088	<u>31.4</u> / <u>.946</u> / .069	<u>31.6</u> / .949 / .068	<u>32.6</u> / .950 / .070	<u>32.6</u> / <u>.952</u> / <u>.066</u>	<u>36.4</u> / <u>.977</u> / <u>.022</u>	28.0 / <u>.919</u> / .114
Ours	4	32.4 / .948 / .070	32.4 / .953 / .062	32.6 / .955 / .060	32.8 / .952 / .066	32.9 / .954 / .063	36.7 / .977 / .021	<u>27.9</u> / .919 / .112
P. ST-4DGS	8	29.1 / .924 / .099	30.0 / .941 / <u>.073</u>	30.6 / <u>.947</u> / <u>.069</u>	30.1 / .883 / .108	31.6 / .947 / .071	33.7 / .968 / .033	27.4 / .916 / <u>.113</u>
P. 4DGS	8	29.6 / <u>.928</u> / <u>.091</u>	29.7 / .937 / .076	30.2 / .940 / .071	<u>32.4</u> / <u>.949</u> / <u>.069</u>	31.6 / .947 / .070	33.8 / .966 / .035	27.3 / .916 / <u>.115</u>
P. Dy.3DGS	8	27.7 / .915 / .117	30.1 / .942 / .074	29.7 / .938 / .082	31.2 / .943 / .079	30.8 / .945 / .073	35.0 / .971 / .032	27.5 / .917 / .115
P. HiCoM	8	<u>29.6</u> / .928 / .102	<u>31.0</u> / <u>.943</u> / .074	<u>31.3</u> / .945 / .075	<u>32.2</u> / .948 / .075	<u>32.1</u> / <u>.950</u> / <u>.069</u>	<u>36.0</u> / <u>.975</u> / <u>.026</u>	28.0 / .918 / .115
Ours	8	31.9 / .944 / .076	31.9 / .951 / .064	32.5 / .954 / .062	32.7 / .952 / .067	32.7 / .953 / .064	36.5 / .976 / .022	<u>27.9</u> / .919 / .112

591
 592 **Update Gaussians and Regularization.** Gaussians are marked
 593 unsolvable in PWI-LS if their V_1 determinant is below 10^{-12} , their
 594 accumulated alpha value is below 10^{-3} , or they cover fewer than 2
 595 pixels. Gaussians are marked unsolvable during multi-view updates
 596 if they are visible in fewer than 2 views, their accumulated alpha
 597 value below 10^{-3} , or covering fewer than 3 pixels across all views.
 598 In the regularization stage, parameters of unsolvable Gaussians are
 599 updated based on their 8 nearest neighbors.
 600

601 **Refinement.** In the refinement stage, Gaussian parameters are
 602 optimized following the original 3DGS method [Kerbl et al. 2023]
 603 for 1,000 iterations without densification.

604 **Runtime.** Our implementation uses PyTorch [Paszke et al. 2017],
 605 Taichi [Hu et al. 2019], CUDA, and the multiprocessing module in
 606 Python to achieve multi-GPU parallel processing. All experiments
 607 run on a server equipped with 8 NVIDIA A100-SXM4-40GB GPUs.

608 5.3 Baseline and Ablation

609 We compare TrackerSplat against representative baseline methods
 610 designed for dynamic scene reconstruction that support Gaussian
 611 trajectory tracking from multi-view videos with fixed camera poses.
 612 The original implementations of these methods do not directly sup-
 613 port multi-GPU parallel processing. Thus, to ensure a fair compari-
 614 son, we carefully copy and refactor their codebases to integrate
 615 them into our parallel framework, strictly preserving their original
 616 designs and hyperparameters to minimize any deviation from their
 617 original implementations:

618 **Parallel HiCoM.** Hierarchical Coherent Motion (HiCoM) [Gao et al.
 619 2024] associates Gaussian motions with distinct regions. In their
 620 open-source code, HiCoM is implemented as a hierarchical grid
 621 with multiple density levels. We copy and adapt this HiCoM grid
 622 implementation to our parallel framework.

623 **Parallel Dynamic 3DGS.** Dynamic 3DGS [Luiten et al. 2024] se-
 624 quentially train Gaussian parameters frame-by-frame with physics-
 625 based regularization. We copy their regularization term and adapt

626 their sequential training to parallel processing by initializing the
 627 training from the first frame of each clip rather than previous frame.
 628 **Parallel 4DGS.** 4DGS [Wu et al. 2024] introduces a deformation field
 629 to represent Gaussian motion. We copy and adapt the deformation
 630 field implementation for parallel processing by training a separate
 631 deformation field per frame, warping Gaussians from the initial
 632 frame to subsequent frames within each clip.

633 **Parallel ST-4DGS.** ST-4DGS [Li et al. 2024c] extends 4DGS by incor-
 634 porating explicit temporal regularization. We copy and adapt their
 635 regularization term to our framework with 4DGS implementation.

636 **TrackerSplat without regularization (Ablation).** As an ablation
 637 study, we remove the regularization stage and directly trained the
 638 Gaussian parameters based on the motion compensation results.

639 All baseline methods share the same initial frame for both short-
 640 clip and long-video experiments.

641 5.4 Comparison of Visual Quality

642 We evaluate rendering quality using three widely accepted metrics:
 643 structural similarity (SSIM), peak signal-to-noise ratio (PSNR), and
 644 perceptual similarity (LPIPS) [Zhang et al. 2018].

645 **Visual quality in short clips:** Table 1 presents quantitative results
 646 from short-clip experiments under different GPU parallelism set-
 647 tings. Existing methods exhibit noticeable quality degradation as
 648 GPU parallelism increases, while our approach maintains higher
 649 visual quality in most cases. For scenes with relatively slow motion
 650 (e.g., "coffee martini" in N3DV), baseline methods experience
 651 only minor quality drops (around 0.1 PSNR), achieving performance
 652 comparable to ours. Figure 5 provides visual comparisons, demon-
 653 strating that baseline methods often struggle with large Gaussian
 654 displacements, causing fading or drifting artifacts in rapidly moving
 655 regions. In contrast, our method better preserves visual fidelity even
 656 in highly dynamic scenes.

657 **Visual quality in long videos:** Figure 4 shows quantitative results
 658 from the long-video experiments. Our method can achieve higher

and more stable visual quality compared to baseline methods in most cases. Rendered videos corresponding to these results are provided in the supplementary material.

5.5 Ablation Study Results

Figure 4 compares results with and without regularization, indicating that motion regularization generally enhances robustness. Nevertheless, in certain scenarios (e.g., "coffee martini"), motion regularization occasionally leads to slight quality reduction. Profiling reveals that regularization effectively corrects outlier Gaussian positions but may also shift already correctly positioned Gaussians, slightly degrading overall quality. For short, robustness of our method against point tracking error stems from several design choices: 1) The point tracking stage provides accurate pixel trajectories in most cases. 2) The PWI-LS step (Sec. 4.3) mitigates individual pixel tracking errors by computing transparency-weighted averages. 3) Multi-view triangulation (Sec. 4.4) corrects trajectory errors by averaging results from multiple viewpoints. 4) Median filtering (Sec. 4.5.1) and propagation (Sec. 4.5.2) handle severe trajectory errors by replacing incorrect trajectories with neighboring Gaussians. 5) The refinement stage (Sec. 4.6) further optimizes Gaussian positions, enhancing final accuracy.

5.6 Comparison of Parallel Performance

Table 2 compares parallel performance across different GPU configurations. TrackerSplat achieves higher throughput in most cases. Our parallel framework can also be readily applied to existing methods, significantly improving their throughput in multi-GPU scenarios. The slower performance of baseline methods is largely due to the computational complexity introduced by their regularization terms or deformation fields. In contrast, although includes additional tracking stages, our method benefits from accurately aligned Gaussians before training, eliminating the need for complex regularization or deformation fields, and thus improving reconstruction throughput. Dynamic3DGS dataset contains more views (27) but at a lower resolution (only 640×360). In this dataset, the increased number of views introduces additional overhead in the point tracking stage. Furthermore, since we uniformly perform 1000 iterations (for baseline training or refinement in TrackerSplat) by randomly sampling views regardless of the total number of available views, the overhead from tracking outweighs the performance gains obtained from simplified training. As a result, our method shows comparatively lower throughput than baselines on this dataset.

6 LIMITATIONS AND FUTURE WORK

Although we successfully exploit point tracking to address the issue that Gaussians cannot reliably compute position gradients for large displacements in dynamic reconstruction, our method still has certain limitations. First, point-tracking models effectively handle large-scale motions but often fail to capture subtle motions of small or thin objects (e.g., human hands or fingers), as these occupy limited regions in input images. This limitation leads to blurred or missing details in subsequent frames, as shown in Figure 5. Second, our method currently lacks mechanisms to correct errors introduced in earlier frames. Consequently, inaccuracies may accumulate and

Table 2. Average throughput comparison (seconds per frame) between TrackerSplat and baseline methods under different GPU parallelism settings (2, 4, and 8 GPUs). Our method achieves the highest throughput in most cases. We also separately report the runtime of the tracking stages (point tracking and motion compensation) and the refinement stage.

Method	GPUs	Dy.3DGS	Meet.Room	st-nerf	N3DV
Parallel ST-4DGS	2	108.9	172.3	181.0	232.1
Parallel 4DGS	2	26.1	42.4	54.9	84.0
Parallel Dyn.3DGS	2	15.8	21.1	36.1	61.6
Parallel HiCoM	2	6.6	<u>13.4</u>	<u>27.0</u>	<u>59.5</u>
Ours (total)	2	<u>7.7</u>	10.7	26.6	55.5
Ours (track+refine)	2	3.9+3.8	2.3+8.4	4.1+22.5	5.9+49.6
Parallel ST-4DGS	4	54.4	86.2	90.5	116.0
Parallel 4DGS	4	13.1	21.2	27.5	42.0
Parallel Dyn.3DGS	4	7.9	10.5	18.0	30.8
Parallel HiCoM	4	3.3	<u>6.7</u>	<u>14.8</u>	<u>29.7</u>
Ours (total)	4	<u>5.2</u>	6.0	13.5	28.1
Ours (track+refine)	4	3.3+1.9	1.7+4.2	2.2+11.3	3.3+24.8
Parallel ST-4DGS	8	27.2	43.1	45.2	58.0
Parallel 4DGS	8	6.5	10.6	13.7	21.0
Parallel Dyn.3DGS	8	4.0	5.3	9.0	15.4
Parallel HiCoM	8	1.6	<u>3.4</u>	<u>7.4</u>	<u>14.9</u>
Ours (total)	8	<u>3.4</u>	3.4	7.1	14.7
Ours (track+refine)	8	2.4+1.0	1.3+2.1	1.5+5.6	2.3+12.4

become increasingly severe over time. Third, typical point tracking methods establish trajectories by matching pixels in subsequent frames with those in the first input frame. Therefore, if an object is fully occluded in the first frame and becomes visible later in a clip, our method may fail to estimate its trajectory correctly, causing incomplete or missing reconstructions.

Potential Solution. Recent studies [Duan et al. 2024; Sun et al. 2024] propose techniques that dynamically remove faded Gaussians and add new ones in regions with high gradients, potentially addressing these limitations. As these methods do not inherently maintain consistent Gaussian trajectories across frames, integrating such techniques with TrackerSplat would require additional mechanisms to match newly added Gaussians to existing trajectories. Exploring this integration represents a promising direction for future research.

7 CONCLUSION

In this work, we introduced TrackerSplat, a novel method for robust and scalable dynamic scene reconstruction using 3DGS. TrackerSplat integrates off-the-shelf point tracking models to extract pixel trajectories, and triangulates them across views to update the position, rotation, and scale of 3D Gaussians. We implement TrackerSplat with a parallel pipeline across 8 GPUs, and evaluate it on real-world dynamic scene datasets. Experimental results demonstrate that TrackerSplat effectively handles large inter-frame displacements and significantly improves reconstruction throughput without sacrificing visual quality. These advancements position TrackerSplat as a scalable and robust solution for dynamic scene reconstruction, paving the way for future real-time applications.

799 REFERENCES

- Jad Abou-Chakra, Krishan Rana, Feras Dayoub, and Niko Suenderhauf. 2024. Physically Embodied Gaussian Splatting: A Visually Learnt and Physically Grounded 3D Representation for Robotics. In *8th Annual Conference on Robot Learning*.
- Carl Doersch, Yi Yang, Mel Vecerik, Dilara Gokay, Ankush Gupta, Yusuf Aytar, Joao Carreira, and Andrew Zisserman. 2023. TAPIR: Tracking Any Point with Per-Frame Initialization and Temporal Refinement. In *Proceedings of the IEEE/CVF International Conference on Computer Vision*. 10061–10072.
- Yuanxing Duan, Fangyin Wei, Qiyu Dai, Yuhang He, Wenzheng Chen, and Baoquan Chen. 2024. 4D-Rotor Gaussian Splatting: Towards Efficient Novel View Synthesis for Dynamic Scenes. In *ACM SIGGRAPH 2024 Conference Papers (SIGGRAPH '24)*. 1–11.
- Zhiwen Fan, Wenyan Cong, Kairun Wen, Kevin Wang, Jian Zhang, Xinghao Ding, Danfei Xu, Boris Ivanovic, Marco Pavone, Georgios Pavlakos, Zhangyang Wang, and Yue Wang. 2024. InstantSplat: Unbounded Sparse-view Pose-free Gaussian Splatting in 40 Seconds. <https://doi.org/10.48550/ARXIV.2403.20309>
- Qiankun Gao, Jiarui Meng, Chengxiang Wen, Jie Chen, and Jian Zhang. 2024. HiCoM: Hierarchical Coherent Motion for Dynamic Streamable Scenes with 3D Gaussian Splatting. In *The Thirty-eighth Annual Conference on Neural Information Processing Systems*.
- Adam W. Harley, Zhaoyuan Fang, and Katerina Fragkiadaki. 2022. Particle Video Revisited: Tracking through Occlusions Using Point Trajectories. In *Computer Vision – ECCV 2022*, Shai Avidan, Gabriel Brostow, Moustapha Cissé, Giovanni Maria Farinella, and Tal Hassner (Eds.), 59–75.
- Yuanming Hu, Tzu-Mao Li, Luke Anderson, Jonathan Ragan-Kelley, and Frédéric Durand. 2019. Taichi: a language for high-performance computation on spatially sparse data structures. *ACM Transactions on Graphics (TOG)* 38, 6 (2019), 201.
- Yi-Hua Huang, Yang-Tian Sun, Ziyi Yang, Xiaoyang Lyu, Yan-Pei Cao, and Xiaojuan Qi. 2024. SC-GS: Sparse-Controlled Gaussian Splatting for Editable Dynamic Scenes. In *Proceedings of the IEEE/CVF Conference on Computer Vision and Pattern Recognition*. 4220–4230.
- Nikita Karaev, Jurii Makarov, Jianyuan Wang, Natalia Neverova, Andrea Vedaldi, and Christian Rupprecht. 2024. CoTracker3: Simpler and Better Point Tracking by Pseudo-Labeling Real Videos. <https://doi.org/10.48550/ARXIV.2410.11831>
- Nikita Karaev, Ignacio Rocco, Benjamin Graham, Natalia Neverova, Andrea Vedaldi, and Christian Rupprecht. 2025. CoTracker: It Is Better to Track Together. In *Computer Vision – ECCV 2024*, Aleš Leonardis, Elisa Ricci, Stefan Roth, Olga Russakovsky, Torsten Sattler, and Gülcin Varol (Eds.), 18–35.
- Bernhard Kerbl, Georgios Kopanas, Thomas Leimkuehler, and George Drettakis. 2023. 3D Gaussian Splatting for Real-Time Radiance Field Rendering. *ACM Transactions on Graphics* 42, 4 (2023), 139:1–139:14.
- Guillaume Le Moing, Jean Ponce, and Cordelia Schmid. 2024. Dense Optical Tracking: Connecting the Dots. In *Proceedings of the IEEE/CVF Conference on Computer Vision and Pattern Recognition*. 19187–19197.
- Jiahui Lei, Yijia Weng, Adam Harley, Leonidas Guibas, and Kostas Daniilidis. 2024. MoScA: Dynamic Gaussian Fusion from Casual Videos via 4D Motion Scaffolds. <https://doi.org/10.48550/ARXIV.2405.17421>
- Deqi Li, Shi-Sheng Huang, Zhiyuan Lu, Xinran Duan, and Hua Huang. 2024c. ST-4DGs: Spatial-Temporally Consistent 4D Gaussian Splatting for Efficient Dynamic Scene Rendering. In *ACM SIGGRAPH 2024 Conference Papers (SIGGRAPH '24)*. 1–11.
- Jiyang Li, Lechao Cheng, Zhangye Wang, Tingting Mu, and Jingxuan He. 2024b. Loop-Gaussian: Creating 3D Cinemagraph with Multi-view Images via Eulerian Motion Field. In *Proceedings of the 32nd ACM International Conference on Multimedia (MM '24)*. 476–485.
- Lingzhi Li, Zhen Shen, Zhongshu Wang, Li Shen, and Ping Tan. 2022a. Streaming Radiance Fields for 3D Video Synthesis. *Advances in Neural Information Processing Systems* 35 (2022), 13485–13498.
- Tianye Li, Mira Slavcheva, Michael Zollhöfer, Simon Green, Christoph Lassner, Changil Kim, Tanner Schmidt, Steven Lovegrove, Michael Goesele, Richard Newcombe, and Zhaoyang Lv. 2022b. Neural 3D Video Synthesis From Multi-View Video. In *Proceedings of the IEEE/CVF Conference on Computer Vision and Pattern Recognition*. 5521–5531.
- Zhan Li, Zhang Chen, Zhong Li, and Yi Xu. 2024a. Spacetime Gaussian Feature Splatting for Real-Time Dynamic View Synthesis. In *Proceedings of the IEEE/CVF Conference on Computer Vision and Pattern Recognition*. 8508–8520.
- Youtian Lin, Zuozhuo Dai, Siyu Zhu, and Yao Yao. 2024. Gaussian-Flow: 4D Reconstruction with Dynamic 3D Gaussian Particle. In *Proceedings of the IEEE/CVF Conference on Computer Vision and Pattern Recognition*. 21136–21145.
- Jonathon Luiten, Georgios Kopanas, Bastian Leibe, and Deva Ramanan. 2024. Dynamic 3D Gaussians: Tracking by Persistent Dynamic View Synthesis. In *3DV*.
- Adam Paszke, Sam Gross, Soumith Chintala, Gregory Chanan, Edward Yang, Zachary DeVito, Zeming Lin, Alban Desmaison, Luca Antiga, and Adam Lerer. 2017. Automatic differentiation in PyTorch. In *NIPS-W*.
- Jenny Seidenschwarz, Qunjie Zhou, Bardienus Duisterhof, Deva Ramanan, and Laura Leal-Taixé. 2025. DynOMo: Online Point Tracking by Dynamic Online Monocular Gaussian Reconstruction. <https://doi.org/10.48550/arXiv.2409.02104>
- arXiv:2409.02104 [cs]
- Ayush Shrivastava and Andrew Owens. 2025. Self-Supervised Any-Point Tracking by Contrastive Random Walks. In *Computer Vision – ECCV 2024*, Aleš Leonardis, Elisa Ricci, Stefan Roth, Olga Russakovsky, Torsten Sattler, and Gülcin Varol (Eds.), 267–284.
- Colton Stearns, Adam Harley, Mikaela Uy, Florian Dubost, Federico Tombari, Gordon Wetzstein, and Leonidas Guibas. 2024. Dynamic Gaussian Marbles for Novel View Synthesis of Casual Monocular Videos. In *SIGGRAPH Asia 2024 Conference Papers*.
- Jiakai Sun, Han Jiao, Guangyuan Li, Zhanjie Zhang, Lei Zhao, and Wei Xing. 2024. 3DGStream: On-the-Fly Training of 3D Gaussians for Efficient Streaming of Photo-Realistic Free-Viewpoint Videos. In *Proceedings of the IEEE/CVF Conference on Computer Vision and Pattern Recognition*. 20675–20685.
- Qianqian Wang, Yen-Yu Chang, Ruojin Cai, Zhengqi Li, Bharath Hariharan, Aleksander Holynski, and Noah Snavely. 2023. Tracking Everything Everywhere All at Once. In *Proceedings of the IEEE/CVF International Conference on Computer Vision*. 19795–19806.
- Qianqian Wang, Vickie Ye, Hang Gao, Jake Austin, Zhengqi Li, and Angjoo Kanazawa. 2024. Shape of Motion: 4D Reconstruction from a Single Video. <https://doi.org/10.48550/ARXIV.2407.13764>
- Guanjun Wu, Taoran Yi, Jiemin Fang, Lingxi Xie, Xiaopeng Zhang, Wei Wei, Wenyu Liu, Qi Tian, and Xinggang Wang. 2024. 4D Gaussian Splatting for Real-Time Dynamic Scene Rendering. In *Proceedings of the IEEE/CVF Conference on Computer Vision and Pattern Recognition*. 20310–20320. arXiv:2310.08528 [cs]
- Zhen Xu, Yinghao Xu, Zhiyuan Yu, Sida Peng, Jiaming Sun, Hujun Bao, and Xiaowei Zhou. 2024. Representing Long Volumetric Video with Temporal Gaussian Hierarchy. *ACM Trans. Graph.* 43, 6 (2024), 171:1–171:18.
- Zeyu Yang, Hongye Yang, Zijie Pan, Xiatian Zhu, and Li Zhang. 2023. Real-Time Photorealistic Dynamic Scene Representation and Rendering with 4D Gaussian Splatting. In *The Twelfth International Conference on Learning Representations*. arXiv:2310.10642 [cs]
- Jiakai Zhang, Xinhang Liu, Xinyi Ye, Fuqiang Zhao, Yanshun Zhang, Minye Wu, Yingliang Zhang, Lan Xu, and Jingyi Yu. 2021. Editable Free-Viewpoint Video Using a Layered Neural Representation. *ACM Transactions on Graphics* 40, 4 (2021), 149:1–149:18.
- Richard Zhang, Phillip Isola, Alexei A Efros, Eli Shechtman, and Oliver Wang. 2018. The Unreasonable Effectiveness of Deep Features as a Perceptual Metric. In *CVPR*.
- Boming Zhao, Yuan Li, Ziyu Sun, Lin Zeng, Yujun Shen, Rui Ma, Yinda Zhang, Hujun Bao, and Zhaopeng Cui. 2024. GaussianPrediction: Dynamic 3D Gaussian Prediction for Motion Extrapolation and Free View Synthesis. In *ACM SIGGRAPH 2024 Conference Papers (SIGGRAPH '24)*. 1–12.
- Xiaoyu Zhou, Zhiwei Lin, Xiaojun Shan, Yongtao Wang, Deqing Sun, and Ming-Hsuan Yang. 2024. DrivingGaussian: Composite Gaussian Splatting for Surrounding Dynamic Autonomous Driving Scenes. In *Proceedings of the IEEE/CVF Conference on Computer Vision and Pattern Recognition*. 21634–21643.

856

857

858

859

860

861

862

863

864

865

866

867

868

869

870

871

872

873

874

875

876

877

878

879

880

881

882

883

884

885

886

887

888

889

890

891

892

893

894

895

896

897

898

899

900

901

902

903

904

905

906

907

908

909

910

911

912

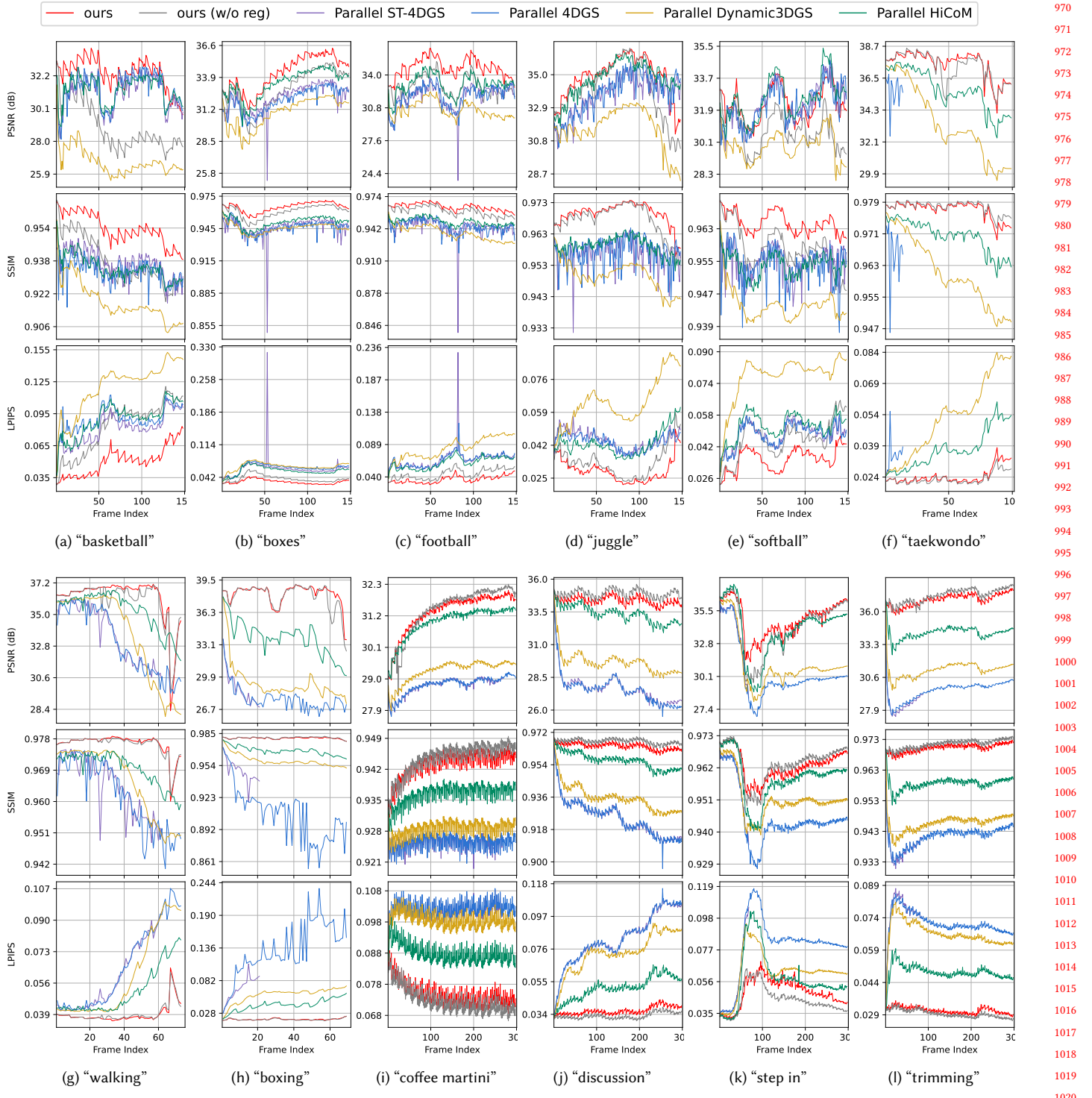


Fig. 4. Average visual quality ($PSNR \uparrow / SSIM \uparrow / LPIPs \downarrow$) over long-video sequences using our parallel pipeline with 8 GPUs (long-video experiments). Our method achieves higher and more stable visual quality than baseline methods in most cases, demonstrating its robustness. Lines ending prematurely for 4DGS and ST-4DGS indicate training failures due to GPU memory overflow (exceeding the 40GB limit of the A100 GPU) or numerical instabilities (NaN gradients). Corresponding rendered videos are provided in the supplementary material.

964
965
966
967
968
969

1021
1022
1023
1024
1025
1026

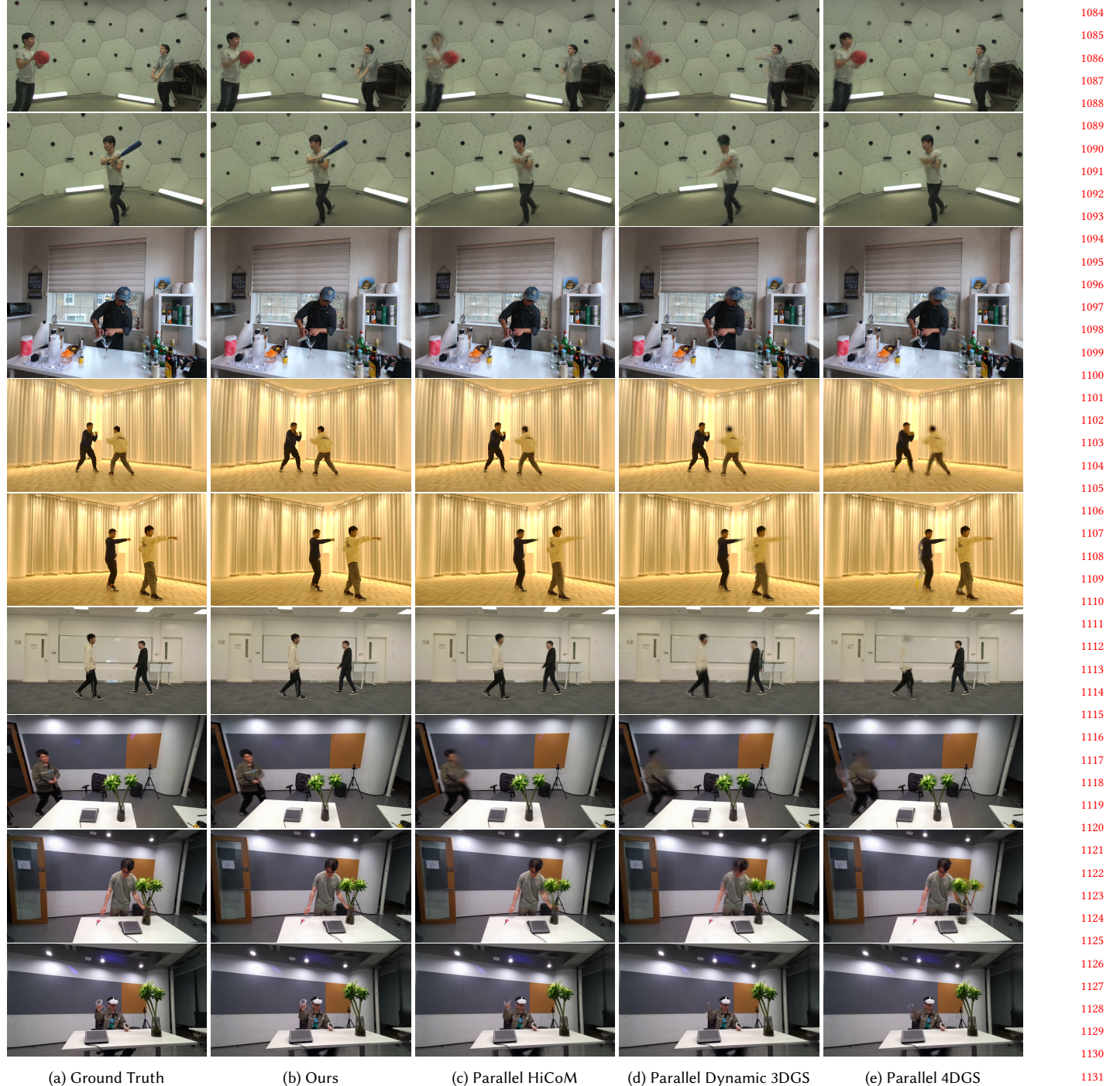


Fig. 5. Qualitative comparison of rendered results from the final frame of representative 9-frame clips processed in parallel using 8 GPUs (short-clip experiments). Our method generates fewer artifacts and better preserves visual details compared to baseline methods, particularly in highly dynamic regions.

1027
1028
1029
1030
1031
1032
1033
1034
1035
1036
1037
1038
1039
1040
1041
1042
1043
1044
1045
1046
1047
1048
1049
1050
1051
1052
1053
1054
1055
1056
1057
1058
1059
1060
1061
1062
1063
1064
1065
1066
1067
1068
1069
1070
1071
1072
1073
1074
1075
1076
1077
1078
1079
1080
1081
1082
1083
1084
1085
1086
1087
1088
1089
1090
1091
1092
1093
1094
1095
1096
1097
1098
1099
1100
1101
1102
1103
1104
1105
1106
1107
1108
1109
1110
1111
1112
1113
1114
1115
1116
1117
1118
1119
1120
1121
1122
1123
1124
1125
1126
1127
1128
1129
1130
1131
1132
1133
1134
1135
1136
1137
1138
1139
1140